Molecular Crystals and Liquid Crystals Science and Technology. Section A. Molecular Crystals and Liquid Crystals

Publication details, including instructions for authors and subscription information:
http://www.tandfonline.com/loi/gmcl19

# Analysis of Shear Flow Effects on Liquid Crystalline Textures

A. D. Rey [a]

[a] Department of Chemical Engineering, McGill University, Montreal, Quebec, Canada, H3A 2A7

Version of record first published: 24 Sep 2006.

To cite this article: A. D. Rey (1993): Analysis of Shear Flow Effects on Liquid Crystalline Textures, Molecular Crystals and Liquid Crystals Science and Technology. Section A. Molecular Crystals and Liquid Crystals, 225:1, 313-335

To link to this article: http://dx.doi.org/10.1080/10587259308036237

*Mol. Cryst. Liq. Cryst.*, 1993, Vol. 225, pp. 313–335
Reprints available directly from the publisher
Photocopying permitted by license only

Printed in the United States of America



# Analysis of Shear Flow Effects on Liquid Crystalline Textures

A. D. REY

*Department of Chemical Engineering, McGill University, Montreal, Quebec, Canada H3A 2A7*

*(Received December 23, 1991)*

A model for the shape and motion of disclination loops observed in thermotropic small molar mass and polymeric nematic liquid crystals in the presence of steady rectilinear shear and oscillatory rectilinear shear flow is presented. In steady rectilinear simple shear, disclination loops elongate and tumble, before retracting to points, in a time that increases with increasing shear rate. In oscillatory shear the loops' shape oscillate with decaying amplitudes between ellipses and circles; the retraction time decreases with increasing frequency. As the driving frequency increases the retraction time decreases. A model for loop population dynamics accounting for the continuous loop creation by surface sources, and loop motion and deformation due to steady rectilinear simple shear predicts that the total number of loops increases with increasing shear rates. The above predictions are in qualitative agreement with experimental results.[5,6] Shear thickening and shear thinning are predicted according to the magnitude of the shear rate and the sensitivity of the initial loop orientation to the strength of the flow.

*Keywords: disclination loops, textures, surface nucleation, shear flow effects*

## 1. INTRODUCTION

Liquid crystalline textures are characterized by the arrangement, number density, dimensionality, character, and strength of defects.[1,2,3] The importance of characterizing and controlling liquid crystalline textures, due to their effect on macroscopic response and physical properties, has recently been emphasized.[4] Most of the research effort in this area focused on molecular structure, surface effects, and thermodynamic variables like pressure, and temperature.[1,2,3] Processing and applications of liquid crystalline materials always involves varying degrees of shear and elongation flow deformations, but details of their effect on the texture parameters remain poorly understood.[2]

The topological similarities and energetic differences of defects in small-molecule liquid crystals (SMLC) and polymeric liquid crystals (LCP) in the absence of flow have been shown to exist.[2] Defect energies affect the number density and spatial mobility of defects, therefore the observed textures in SMLC and LCP are expected to be different, but the topological similarities imply the presence of defects of the same dimension and strength in both types of materials. For example, thermotropic nematic SMLC and LCP both exhibit disclination singular lines of strength S =

$\pm 1/2$ (thins), coreless disclinations of integral strength $S = \pm 1$ in the form of loops or attached to the surfaces or other line segments, singular points, and inversion walls.[2] In both materials the stress fields generated by these defects produce relative motions and interactions among them, with the result that textures are continuously changing with a dynamics that depends on the viscosities involved in the defect motions. For example, disclination loops of strength $S = +1/2$, are known to shrink, due to their line tension, into singular points of the same topological charge with a characteristic retraction time that scales with the inverse of the rotational viscosity.

Shear flow is an important instance where, despite the noted energetic differences of defects between thermotropic nematic SMLC and thermotropic nematic LCP, the observed textures exhibit important similarities. Detailed experimental rheoptical studies of thermotropic nematic SMLC[5] and main chain thermotropic nematic LCP[6] in shear flows between concentric discs show, in both instances, that at a critical shear rate there is a profound textural change characterized by the presence of a high density of disclination loops. In the case of MBBA, a thermotropic nematic SMLC, in steady circular shear flow, it is reported that these loops may have singular cores of strength $\pm 1/2$ (thins), or they can be coreless with integral strength $\pm 1$ (thicks). Thicks are formed in the bulk of the flowing liquid, around debris in the material but sometimes without the visible presence of a nucleation site. Thins nucleate on the boundaries and migrate into the bulk. The loops tumbled, deformed, and shrunk in the flow, and the loop population was maintained by a continuous nucleation that increased with increasing shear rate. For the case of a series of main chain thermotropic nematic LCP's in oscillatory shear flows between circular discs it is reported that at a critical shear rate a massive multiplication of disclination loops occurs. Increasing the frequency (shear rate) refines the texture by shrinkage of the characteristic loop size, and at sufficiently large shear rates no loops appear in the field of vision of an optical microscope.

The nucleation of disclinations in the bulk at a critical field strength by pinching of inversion walls has been considered for the periodic twist Fredericks transition in nematic LCP's[7] and electrohydrodynamic instabilities[8] in SMLC nematics. In these models the texture dynamics evolves by bulk nucleation and interaction of singular disclination pairs of opposite signs; in these models the total length of disclination lines only changes by the balance of creation and annihilation of disclination pairs. Several theoretical models for various textured LCP materials have been presented[9-13]; although the above models are successful in predicting important rheological properties they seem not to include the possibility of textural changes by surface defect nucleation at some critical deformation rate, as observed in the materials described in the previous paragraph. The effects of structural defects on the rheology of lyotropic lamelar phases has been analyzed for shear flow[14]; here the presence of a large density of undeformable rigid dislocation loops explains the large viscosity increase observed near the isotropic transition, but since loops are considered undeformable the texture is not affected by the flow deformation.

The objective of this paper is to provide an analysis of the effects of shear flow on optical textures of thermotropic liquid crystalline materials, as reported by References 5 and 6. Without loss of generality the shear flows considered here are

steady rectilinear simple shear and oscillatory rectilinear shear. The texture in this paper is characterized by a number density of singular disclination loops of strength $S = \pm 1/2$ (thins) that deform and tumble in the flowing material. As reported in the experiments,[5] the loops considered in this paper nucleate at the surface at a critical shear rate, and as the shear rate increases its nucleation rate increases. As the loops adopt an orientation parallel to the bounding surfaces they quickly shrink, so that the actual loop density is given by a loop population balance between shrinking deformable loops and continuously created loops. The system is taken to be a suspension of noninteracting elastic loops in a Newtonian isotropic fluid matrix. In this paper we show how a single loop deforms, moves, and collapses into a point in steady and oscillatory shear, and later we model the effect of steady shear on a deformable loop population, accounting for the continuous birth by surface nucleation and death by shrinkage into points.

The basic concepts for retraction of disclination loops in the absence of flow are given in section 2. Section 3 presents a balance equation for a single loop motion, size and shape in steady shear flow. Section 4 treats the effect of the frequency of an oscillatory shear flow on a single disclination loop shape, size, and motion. Section 5 applies a loop population balance in the presence of a steady shear flow. This section incorporates a model given previously for the nucleation rate of disclination loops in the steady shear flow of nematics.[15] The total number of loops and characteristic size as a function of shear rate are derived from the loop density taking the loop orientation at the nucleation site as a parameter. Finally the effect of the texture on the viscosity is estimated.

## 2. LOOP DYNAMICS IN THE ABSENCE OF FLOW

The basic phenomena of a single disclination loop in the absence of macroscopic externally imposed flows is given in References 15 and 16. A disclination loop of radius $r$ tends to shrink due to the line tension $\Gamma$ that gives rise to a radial force per unit length $-\Gamma/r$. The retraction of the loop is balanced by a viscous drag $\xi\, dr/dt$; $\xi$ is the line friction coefficient given by $\xi = \Gamma/D$ and the orientation diffusivity $D$ is given the ratio of a characteristic Frank elastic constant $K$ and the rotational viscosity $\gamma_1$, $D = K/\gamma_1$. Integrating the force balance $r\, dr/dt = -D$ gives:

$$r^2 = r_0^2 - 2Dt \tag{1}$$

where $r_0$ is the initial loop radius. The loop retracts in a time $\tau = r_0^2/2D$; if the loop has a strength $S = +1/2$ it collapses to a point defect of the same strength, but if the loops consisted of pieces of disclinations of strength $S = \pm 1/2$ it will not leave a point singularity.

If we now have a surface source emitting $B'$ loops per unit time of radius $r_0$ the

loop population balance governing the loop density per unit radial length $n(r)$, in dimensionless form, is given by:

$$\frac{\partial n}{\partial t^*} + \frac{\partial}{\partial r^*}\left(\frac{dr^*}{dt^*} n\right) = 0 \tag{2}$$

where $t^* = tD/r_0^2$, and $r^* = r/r_0$; diffusion in size space is assumed to be negligible when compared to convection. In Equation (2) $n(r)\,dr$ is the number of loops with a radius between $r$ and $r + dr$. The initial and boundary conditions are:

$$t^* = 0, \quad 0 \leqslant r^* \leqslant 1, \quad n(r^*, 0) = 0 \tag{3a}$$

$$r^* = 1, \quad t^* > 0, \quad n(1, t^*) = BU(t^*) \tag{3b}$$

where B are the number of loops of unit radius emitted per unit time, and $U(t)$ is the Heaviside function: $U(t^*) = 1$ for $t^* \geqslant 0$, and $U(t^*) = 0$ for $t^* < 0$. Equation (2) is solved by the method of characteristics; the characteristics are given by $t^* = -r^{*2}/2 + \varepsilon$, where $\varepsilon$ defines each characteristic. Using Equation (1), the solution of (2) satisfying (3) is:

$$n(r^*, t^*) = BrU\left(t^* + \frac{r^{*2}}{2} - \frac{1}{2}\right) \tag{4a}$$

which describes the stepwise formation of a linear loop density profile by a left moving front of speed $dr^*/dt^* = 1/r^*$; after $t^* \geqslant 1/2$ the steady loop density is:

$$n(r^*) = Br^* \tag{4b}$$

Integrating the loop density $n(r^*, t^*)$ gives the total number of loops $N(t^*)$ due to the source $B$:

$$N(t^*) = \int_0^1 n(r^*, t^*)\, dr^* = Bt^*, \; t^* \leqslant 1/2 \tag{5a}$$

which reaches the stationary value $N = B/2$ at $t^* = 1/2$; the average perimeter $\langle P^* \rangle = 2\pi \langle r^*(t^*) \rangle$ is given by:

$$\langle P^*(t^*) \rangle = \frac{2\pi}{N} \int_0^1 n(r^*, t^*) r^*\, dr^* = \frac{2\pi}{3t^*}\left[1 - (1 - 2t^*)^{3/2}\right], \quad t^* \leqslant 1/2 \tag{5b}$$

and reaches the stationary value $\langle P^* \rangle = 4\pi/3$ at $t^* = 1/2$. The above analysis is given on a per source basis; if there are $C$ active source per unit volume each emitting $B$ loops of radius $r^* = 1$ per unit time, the total number of loops per unit volume is $C \times N$.

The presence of a shear flow will modify all the above results since loops will

experience the combined action of flow torques and forces due to the vorticity and extention-compression effects of a simple shear flow.

## 3. SINGLE LOOP DYNAMICS IN STEADY SIMPLE SHEAR FLOW

In this section we derive the equations governing the motion and shape of a single loop in the presence of rectilinear steady simple shear flor between two flat plates. We assume, as in the rest of this paper that the shape of the loop is described at all times by an ellipse whose semiaxes define a plane normal to the shear plane, where the shear plane is defined by the flow direction and the normal to the bounding parallel surfaces, as shown in Figure 1. The loop is assumed to be circular initially, with a center of mass always travelling with the same velocity as the fluid, to tumble affinely due to the vorticity, and to deform due to the flow forces, as reported in Reference 5 for the case of 4-methoxy-benzylidene-4′-*n*-butylaniline (MBBA), a thermotropic nematic SMLC, in steady shear.

The affine rotation of the loop due to the vorticity of the flow is specified by the rotation speed of a unit vector **n** in the direction of the semiaxis **a**, which always lies in the shear plane:

$$\dot{\mathbf{n}} = (\mathbf{P}\cdot\mathbf{S})\cdot\mathbf{n} \tag{6}$$

where **P** is the projection operator **P** = (**I**-**nn**), **S** is the velocity gradient tensor,

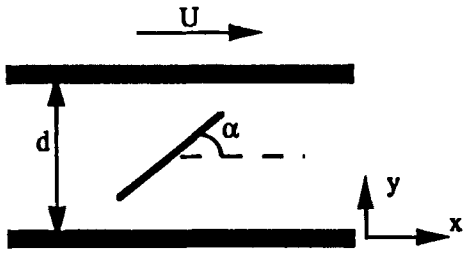


(a)

FIGURE 1a Definition of flow geometry, coordinate system, and side view of a disclination loop. α is the angle of the semiaxis **a** with the flow direction (*x*).

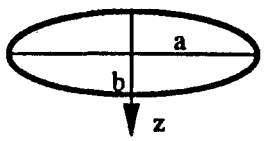


(b)

FIGURE 1b Corresponding normal view of a disclination loop. The semiaxis of the loop along the *z*-direction is **b** = (0, 0, *b*), and **a** = ($a_x$, $a_y$, 0) is the semiaxis of the loop in the shear plane (*x*-*y*).

and a superposed dot denotes time differentiation. For the present case $\mathbf{n} = (\cos \alpha, \sin \alpha, 0)$, and the only nonzero component of $\mathbf{S}$ is $S_{xy} = \gamma$, where $\gamma$ is the shear rate given by the ratio of the upper plate velocity $U$ and the plate separation $d$, $\gamma = U/d$. The loop rotates affinely due to the vorticity of the flow with an angular velocity given by:

$$\dot{\alpha} = -\gamma \sin^2 \alpha \tag{7}$$

Integration of (7) gives the loop orientation as a function of time:

$$\cot \alpha = \gamma t + \cot \alpha_0 \tag{8}$$

where $\alpha_0$ is the initial loop orientation, restricted by $\pi \leqslant \alpha_0 \leqslant 0$.

The shape of the ellipse is given by the equation of motion of the two semiaxis vectors $\mathbf{a}$ and $\mathbf{b}$, where $\mathbf{a}$ always lies in the $x$-$y$ plane and $\mathbf{b}$ is always directed along the neutral $z$-axis. Neglecting inertia there is a viscous drag force balancing an elastic force from the elastic line tension of the loop:

$$\zeta(\dot{\mathbf{a}} - \mathbf{S}\cdot\mathbf{a}) = -\mathbf{F}^{e,a} \tag{9a}$$

$$\zeta(\dot{\mathbf{b}} - \mathbf{S}\cdot\mathbf{b}) = -\mathbf{F}^{e,b} \tag{9b}$$

where $\zeta = \Gamma\gamma_1/K$ is the line friction coefficient above, and the right hand sides represent the elastic forces acting on the loop along the directions of the semiaxes $\mathbf{a}$ and $\mathbf{b}$, respectively. As in the case of circular loops[15] the elastic forces are given by the ratio of the line tension $\Gamma$ and the local radius of curvature $\rho$,[17] as follows:

$$\mathbf{F}^{e,a} = \frac{\Gamma}{\rho_a}\frac{\mathbf{a}}{|\mathbf{a}|} = \frac{a\Gamma}{b^2}\frac{\mathbf{a}}{|\mathbf{a}|} \tag{10a}$$

$$\mathbf{F}^{e,b} = \frac{\Gamma}{\rho_b}\frac{\mathbf{b}}{|\mathbf{b}|} = \frac{b\Gamma}{a^2}\frac{\mathbf{b}}{|\mathbf{b}|} \tag{10b}$$

where $a$ and $b$ denote the magnitudes of $\mathbf{a}$ and $\mathbf{b}$, respectively. A large stretching of the semiaxis $a$ produces a large restoring elastic force along $\mathbf{a}$ but reduces the retraction along $\mathbf{b}$, and since $\mathbf{b}$ lies along the neutral direction its magnitude will monotonically decrease at all times. Replacing Equations (10) into (9) we obtain for the present shear flow ($\mathbf{S}\cdot\mathbf{b} = \mathbf{0}$):

$$\dot{\mathbf{a}} = \mathbf{S}\cdot\mathbf{a} - D\frac{a}{b^2}\frac{\mathbf{a}}{|\mathbf{a}|} \tag{11a}$$

$$\dot{\mathbf{b}} = -D\frac{b}{a^2}\frac{\mathbf{b}}{|\mathbf{b}|} \tag{11b}$$

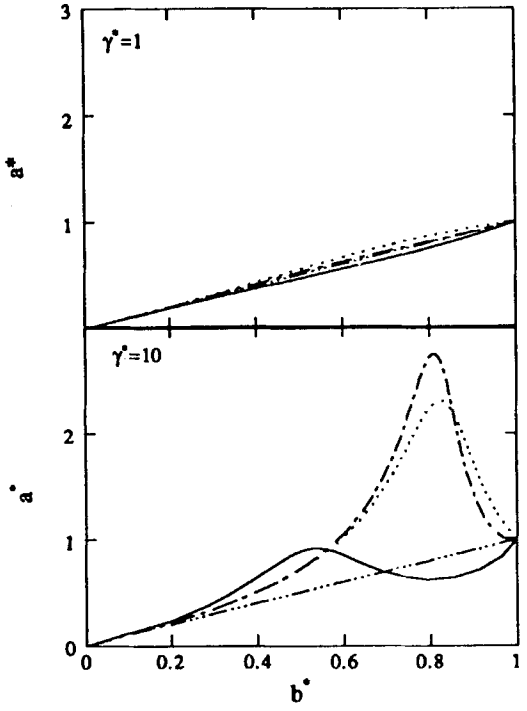


FIGURE 2 Evolution of the dimensionless semiaxis $a^*$ as a function of $b^*$, in steady simple rectilinear shear flow, for two shear rates $\gamma^* = 1$ (top) and $\gamma^* = 10$ (bottom), and four initial orientations $\alpha_0$: $3\pi/4$ (full), $\pi/2$ (dash dot), $\pi/4$ (dash), and 0 (dash-triple dot).

where $D = K/\gamma_1$ is the orientation diffusivity defined above. The scalar dimensionless equations of motion for $a$ and $b$, obtained by dotting (11a) with **a** and noting that $\mathbf{b} = (0, 0, b)$, are given by:

$$\frac{da^*}{dt^*} = \frac{\gamma^* a^* (\gamma t^* + \cot \alpha_0)}{[1 + (\gamma t^* + \cot \alpha_0)^2]} - \frac{a^*}{b^{*2}} \tag{12a}$$

$$\frac{db^*}{dt^*} = -\frac{b^*}{a^{*2}} \tag{12b}$$

where $a^* = a/r_0$, $b^* = b/r_0$, $t^* = tD/r_0^2$, and $\gamma^* = \gamma r_0^2/D$; in Equation (12a) we replaced $\sin \alpha \cos \alpha$ using Equation (8).

The loop shape $(a^*(t^*), b^*(t^*))$ and orientation $(\alpha(t^*))$ are given by the solution to Equations (8) and (12). These equations were solved using an implicit corrector-predictor Euler method with adaptable time integration step,[18] and the following initial conditions:

$$t^* = 0, \quad a^* = b^* = 1 \tag{13}$$

A parametric study was performed on the initial circular loop orientation $\alpha_0$ and

the shear rate $\gamma^*$. The representative values for the initial orientation were chosen as: $\alpha_0 = 3\pi/4, \pi/2, \pi/4, 0$, and for the shear rate $\gamma^* = 1, 10$. Taking $r_0 = 5$ μm, and $D = 10^{-6}$ cm$^2$/sec as representative of nematic SMLC the relation between scales are: $\gamma^* = \gamma/4$, $t^* = 4t$.

Figure 2 shows the evolution of the loop semiaxes $a(t^*)$ and $b(t^*)$, for four initial orientations and two shear rates. At $t^* = 0$, $a^* = b^* = 1$ and as time passes the semiaxes retract at different rates, giving rise to different elliptic loops according to the initial orientation. At low shear rate ($\gamma^* = 1$) $\alpha_0$ has no significant effect on the ellipticity of the loop, and the loop retracts to a point always maintaining the circular shape, given by the line $a^* = b^*$. At higher shear rates ($\gamma^* = 10$) there is a significant effect of the initial loop orientation. Loops initially in the extension quadrant ($0 \leq \alpha \leq \pi/2$) of the shear flow experience a significant stretching and they retract as an elongated ellipse $a^* > b^*$. Loops initially parallel to the bounding surfaces ($\alpha_0 = 0$) are not affected by the flow and retract as circles with $a^* = b^*$, as shown in section 2. Loops initially in the compression quadrant ($\pi \geq \alpha \geq \pi/2$) of the shear flow experience a faster shrinkage in $a^*$ than $b^*$ until the loop enters the extension quadrant and then it retracts with $a^* > b^*$. Figure 3 shows the corresponding loop orientation as a function of time. At low $\gamma^*$ the loops retract without significant rotation, while at larger $\gamma^*$ the loops sample large angular sectors before collapsing to points. Figure 4 shows the corresponding perimeters as a function of time. The perimeters are given by $P^* = 2\pi\,((a^{*2} + b^{*2})/2)^{1/2}$. At low $\gamma^*$ there is no significant flow effect, while at larger $\gamma^*$ the perimeter corresponding to loops initially in the extension quadrant exhibit a maxima at $t^*$

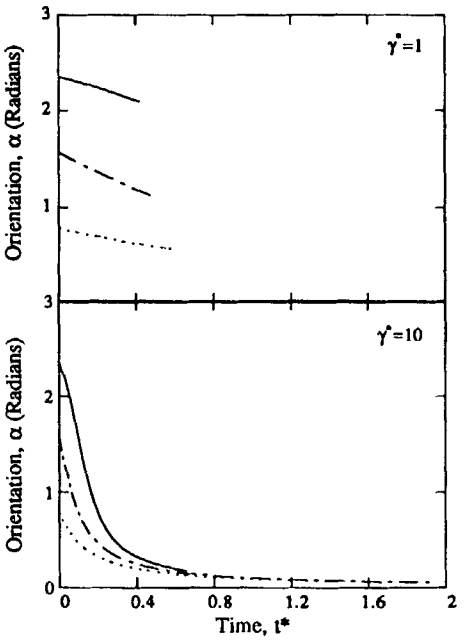


FIGURE 3 Loop orientation α (radians) as a function of time $t^*$ for the same conditions as in Figure 2.

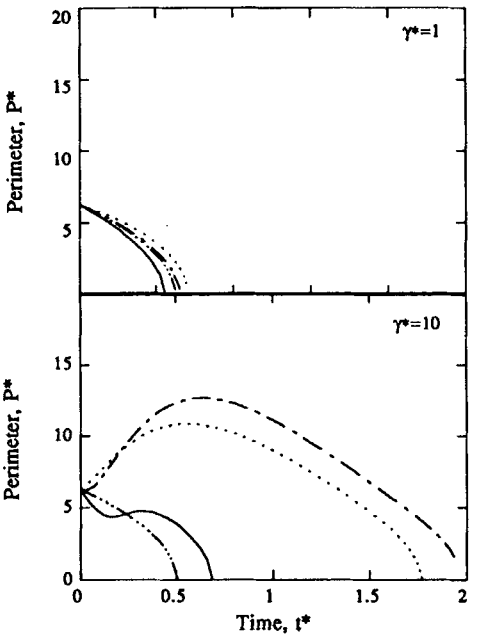


FIGURE 4 Loop perimeter $P^*$ as a function of time $t^*$ for the same conditions as in Figure 2.

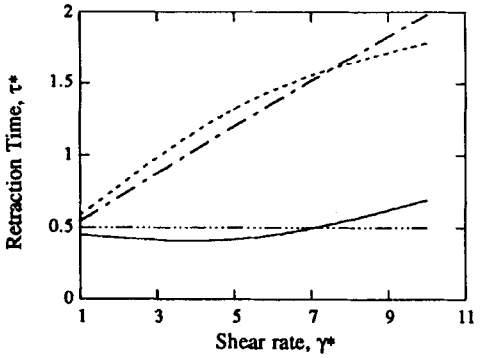


FIGURE 5 Retraction time $\tau^*$ as a function of shear rate $\dot{\gamma}^*$. The retraction time is the time required for $a^* = b^* = 0$.

$> 0$, while the others decrease monotonically ($\alpha_0 = 0$) or with damped oscillations ($\alpha_0 = 3\pi/4$).

The retraction time $\tau^*$ as a function of shear rate is shown in Figure 5. Only loops initially in the extension quadrant exhibit a significant increase in their retraction time as shear rate increases; loops initially parallel to the bounding surfaces quickly retract, independently of the imposed shear flow strength following the dynamics shown in section 2.

The simple model presented here predicts that loops initially in the extension quadrant of the shear flow tumble and elongate along the flow direction before shrinking to a point, and their retraction times increase with increasing shear rates,

in qualitative agreement with experimental observations.[5] Loops initially parallel to the surfaces quickly retract with circular shapes independently of $\gamma^*$, as shown above. Loops initially in the compression quadrant retract as nearly circular ellipses.

## 4. SINGLE LOOP DYNAMICS IN OSCILLATORY SHEAR FLOW

In this section we derive the equations governing the motion and shape of a single disclination loop in the presence of oscillatory shear flow between two flat plates. A detailed experimental study using various random copolyester thermotropic mainchain nematic LCP's in oscillatory shear flow shows that at a critical maximum shear rate of the cycle there is a massive nucleation of disclination loops, and that as the maximum shear rate (frequency) increases the characteristic loop size decreases until the microscope is unable to detect their presence.[6] In this section we treat a single loop dynamics and explore the effect of increasing the maximum shear rate on the loop shape, orientation, retraction time, and perimeter.

For rectilinear oscillatory shear the displacement $x$ of upper plate shown in Figure 1 is taken to be $x = A\cos(\omega t)$, and the shear rate across the gap is given by:

$$\gamma = \gamma_0 \cos(\omega t) \tag{14}$$

where $\gamma_0$ is the magnitude of the maximum shear rate $\gamma_0 = A\omega/d$, where $A$ is the amplitude and $d$ the plate spacing. Replacing Equation (14) into (7) gives the angular velocity of the loop as:

$$\dot{\alpha} = -\gamma_0 \cos(\omega t)\sin^2 \alpha \tag{15}$$

Integration of (15) gives the loop orientation as a function of time:

$$\cot \alpha = \frac{\gamma_0}{\omega} \sin(\omega t) + \cot \alpha_0 \tag{16}$$

where $\alpha_0$ is the initial loop orientation, restricted by $\pi \leqslant \alpha_0 \leqslant 0$.

Proceeding exactly as in the previous section, using Equations (9, 11, 16) and $S_{xy} = \gamma_0 \cos(\omega t)$, we obtain the following dimensionless equations governing the semiaxes $a^*$ and $b^*$:

$$\frac{da^*}{dt^*} = \frac{a^*\left(\cot \alpha_0 \gamma_0^* \cos(\omega t^*) + \dfrac{\gamma_0^{*2}}{2w^*} \sin(2\omega^* t^*)\right)}{1 + \left(\cot \alpha_0 + \dfrac{\gamma_0^*}{\omega^*} \sin(\omega^* t^*)\right)^2} - \frac{a^*}{b^{*2}} \tag{17a}$$

$$\frac{db^*}{dt^*} = -\frac{b^*}{a^{*2}} \tag{17b}$$

where $a^* = a/r_0$, $b^* = b/r_0$, $t^* = tD/r_0^2$, $\omega_0^* = \omega_0 r_0^2/D$, and $\gamma_0^* = \gamma_0 r_0^2/D$.

The loop shape $(a^*(t^*), b^*(t^*))$ and orientation $(\alpha(t^*))$ are given by the solution to Equations (16) and (17). These equations were solved using the same numerical method described above, with the following initial conditions:

$$t^* = 0, \quad a^* = b^* = 1 \tag{18}$$

A parametric study was performed on the initial circular loop orientation $\alpha_0$ and the angular frequency $\omega^*$. The representative values for the initial orientation were chosen as: $\alpha_0 = 3\pi/4, \pi/2, \pi/4, 0$, and for angular frequency $\omega^* = 0.1, 1, 10, 100$. Taking $r_0 = 1\ \mu m$, $d = 2\ \mu m$ $A = 0.02$ cm, and $D = 5\,10^{-8}$ cm$^2$/sec as representative of a nematic LCP, the relations between scales are: $\gamma_0^* = \gamma_0/5$, $w^* = w/5$, $t^* = 5t$, and $\gamma_0^* = 100\omega^*$. In what follows large (small) angular frequencies $\omega^*$ denote large (small) magnitudes of the maximum shear rates $\gamma_0^*$.

Figure 6 shows the evolution of the loop semiaxes $a(t^*)$ and $b(t^*)$, for four initial orientations and three angular frequencies. At $t^* = 0$, $a^* = b^* = 1$, and as time passes the semiaxes retract at different rates, giving rise to different elliptic loops according to the initial orientation. Since the flow is oscillatory the extension and compression quadrants change with the sign of $\gamma^*$, and the semiaxis **a** may sample a series of extensions and compressions if the loop retraction time $\tau^*$ is sufficiently larger than $(d\alpha/dt^*)^{-1}$. At low frequencies ($\omega^* = 0.1$) $\alpha_0$ has no significant effect on the ellipticity of the loop, and the loop retracts to a point always maintaining the circular shape, given by the line $a^* = b^*$. At intermediate frequencies ($\omega^* = 1$) there is a significant effect of the initial loop orientation. Loops initially in the extension quadrant ($0 \leqslant \alpha \leqslant \pi/2$) of the shear flow remain in this quadrant, experience a significant stretching and retract as an elongated ellipse $a^* > b^*$. Loops initially parallel to the bounding surfaces ($\alpha_0 = 0$) are not affected by the flow and retract as circles with $a^* = b^*$, as shown in section 2. Loops initially in the compression quadrant ($\pi \geqslant \alpha \geqslant \pi/2$) of the shear flow experience a faster shrinkage in $a^*$ than $b^*$ until the loop enters the extension quadrant and then retracts with $a^* > b^*$. At higher frequencies ($\omega^* = 10$) the orientation of the loops periodically sample both the stretching and compression quadrants and they retract with a shape that oscillates periodically, with loss of amplitude, between an ellipse and a circle, before collapsing into a point.

Figure 7 shows the corresponding loop orientation as a function of time. At low $\omega^*$ the loops retract without significant rotation, at intermediate $\omega^*$ the loops rotate but always remain in the first quadrant, while at large $\omega^*$ the loops sample the first and second quadrants before collapsing to points.

The three upper plots in Figure 8 show the corresponding perimeters as a function of time, and the lower plot for $\omega^* = 100$. At $\omega^* = 0.1$ there is no significant flow effect on $P^*$, while at $\omega^* = 1$ the perimeter of loops initially in the extension quadrant exhibit a maxima at $t^* > 0$, while the others decrease monotonically ($\alpha_0 = 0$) or with damped oscillations ($\alpha_0 = 3\pi/4$). At $\omega^* = 10$ the perimeters of loops not parallel to the surfaces oscillate with loss of amplitude; after each period the loops return to the circular shape and the maximal perimeters occur when the loops are almost parallel to the bounding surfaces. At very high frequency, $\omega^* = 100$, the period of the oscillations is set by $\omega^*$, the elliptical loop shapes pulsate around the shrinking circle corresponding to the loop initially parallel to the plates.

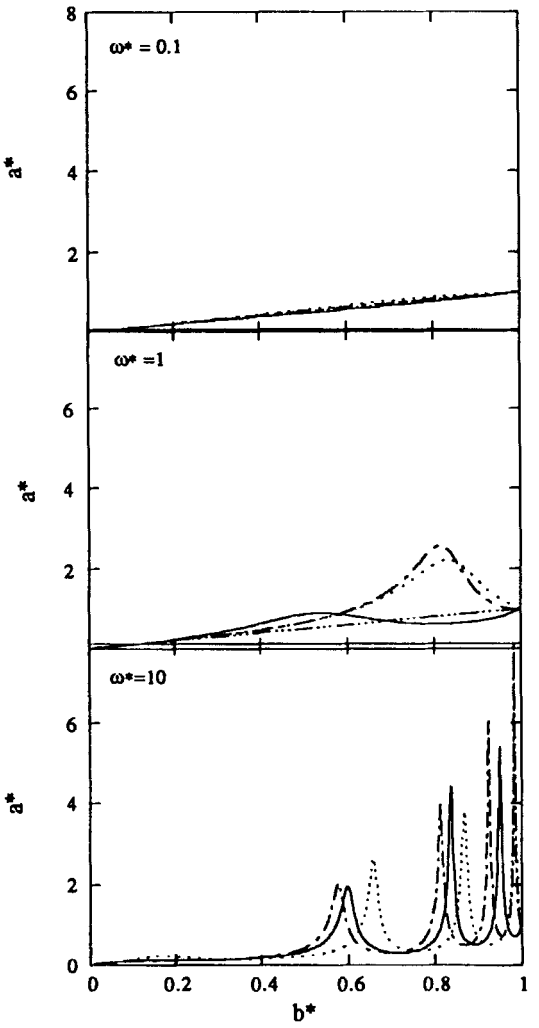


FIGURE 6 Evolution of the dimensionless semiaxis $a^*$ as a function of $b^*$, in oscillatory rectilinear shear, for three angular frequencies $\omega^* = 0.1$ (top), $\omega^* = 1$ (middle), and $\gamma^* = 10$ (bottom), and four initial orientations $\alpha_0$: $3\pi/4$ (full), $\pi/2$ (dash dot), $\pi/4$ (dash), and 0 (dash-triple dot). The relation between frequency and shear rate is $\gamma^* = 100\omega^*$.

Figure 9 shows the damped oscillatory evolution of the perimeter $\langle P^* \rangle$ on the right vertical scale, and the angle $\alpha$ and $\cos(wt^*)$ on the left vertical scale, for $\alpha_0 = 3\pi/4$ and $\omega^* = 10$. The vertical lines denote the time at which the shear rate changes sign, and E(C) stands for extension (compression) of the **a** axis. The figure shows that **a** exhibits an extension (compression) when the angle of $a$ and the positive flow direction is less (more) than $\pi/2$. The shrinkage of the loop therefore is given by periodic oscillations with continuous loss of amplitude.

Figure 10 shows the retraction time $\tau^*$ as a function of frequency for four initial orientations. For loops initially oriented parallel to the surfaces $\tau^*$ is independent of $\omega^*$, and the loop retract as circles, $a^* = b^*$, exactly as in section 2. For any

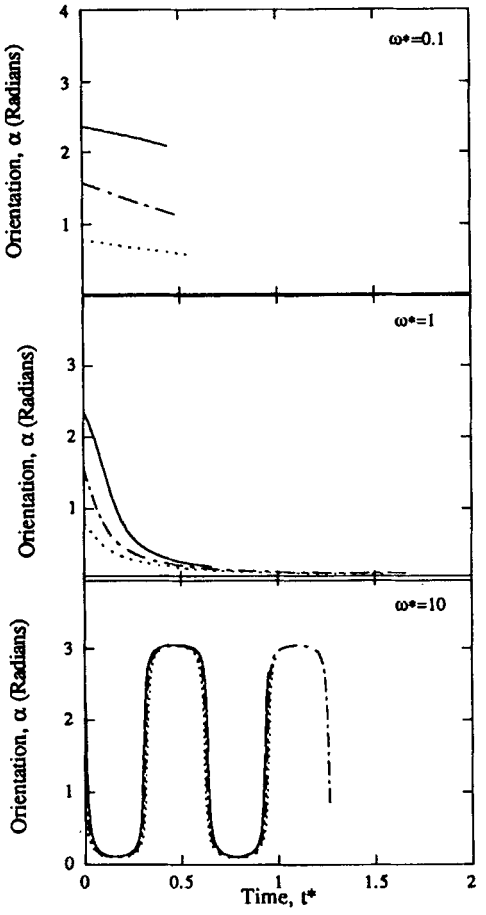


FIGURE 7 Loop orientation α (radians) as a function of time $t^*$ for the same conditions as in Figure 6.

other initial orientation increasing $\omega^*$ decreases $\tau^*$, and at sufficiently high frequencies the loops will shrink even faster than in the absence of flow.

In this section we have shown that for sufficiently high frequencies the effect of an oscillatory shear flow on the retraction time, and mode of shrinking of a disclination loop is significantly different than that of a steady shear flow. For sufficiently high frequencies the net effect of the periodic extensions and compressions of the semiaxis **a** results in a faster retraction than that of a loop in the absence of flow. This observation is in qualitative agreement with experimental results,[6] where it is reported that at sufficiently high frequencies the optical microscope is unable to detect the presence of any loops.

## 5. LOOP POPULATION DYNAMICS IN SIMPLE SHEAR FLOW

The objective of this section is first to show that the profound textural change during the shear flow of thermotropic SMLC and LCP when the shear rate in the

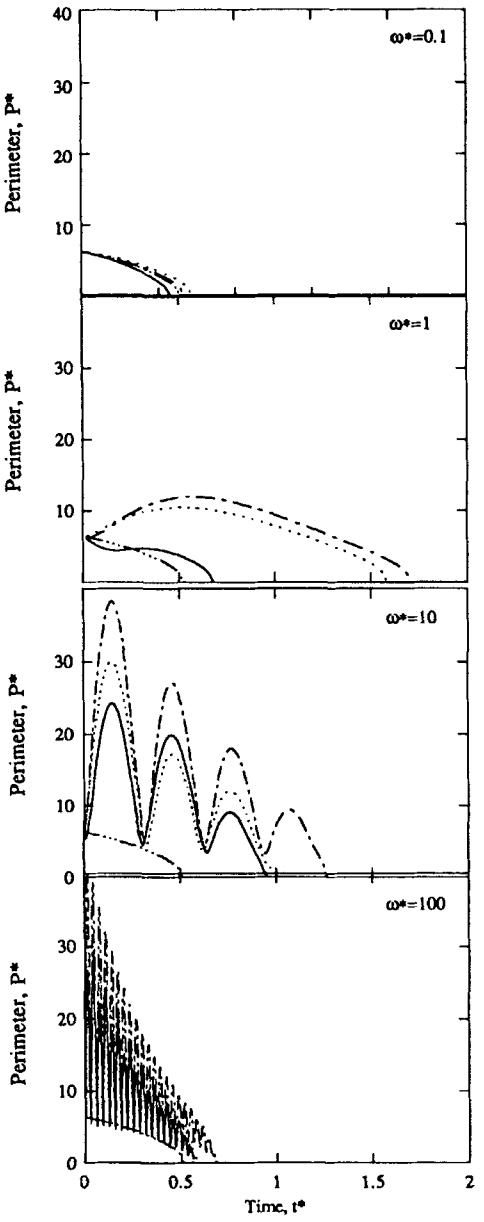


FIGURE 8 Loop perimeter $P^*$ as a function of time $t^*$ for the same conditions as in Figure 6. The bottom graph shows the behaviour for the same initial orientations at a very high frequency $\omega^* = 100$.

steady shear or the maximum shear rate in oscillatory reaches a critical value can be explained by a model presented previously.[15] In both instances and for both materials it is reported that a massive density of disclination loops suddenly appears in the field of vision when the strongly sheared sample is observed with an optical microscope.[6] In this section we also present a simple loop population model for

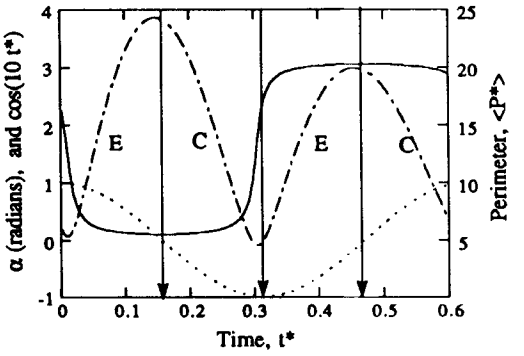


FIGURE 9 Couplings between rotation, deformation, and oscillatory shear, for $\omega^* = 10$. The full line denotes the loop orientation $\alpha$ as a function of time $t^*$, measured on the left vertical scale. The dotted line, $\cos(10t^*)$, is proportional to the shear rate. The dash dot line is the average perimeter $\langle P^* \rangle$ measured on the right vertical scale. E(C) denotes extension (compression).

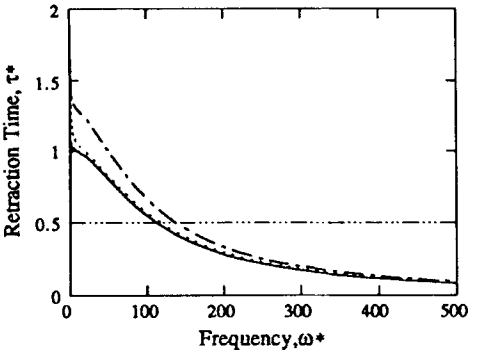


FIGURE 10 Retraction time $\tau^*$ as a function of angular frequency $\omega^*$ for four initial orientations $\alpha_0$: $3\pi/4$ (full), $\pi/2$ (dash dot), $\pi/4$ (dash), and 0 (dash-triple dot).

steady simple shear that accounts for the continuous nucleation, deformation and tumbling, and shrinkage of disclination loops, modelled as elastic strings suspended in a Newtonian fluid.

Besides bulk nucleation of disclination pairs by wall pinching,[7] loop emission by pinned disclination segments at the bounding surfaces is another likely mechanism to affect the texture of a liquid crystalline material. A model of loop emission, by pinned disclination segments at the bounding surfaces in a simple shear flow has been presented in Reference 15. This model, analogous to the Frank-Read model for dislocations in metals,[19] predicts that at a critical shear rate $\gamma_c$, the line tension force of a pinned disclination segment is unable to balance the viscous drag force of a shear flow, and the line will emit loops at regular intervals. An approximate balance of forces along the flow direction gives the critical shear rate as:

$$\gamma_c = \frac{2D}{Lb} \tag{19}$$

where $D$ is the orientation diffusivity, $L$ is the distance between anchoring points of the disclination line segment, and $b$ is the maximum distance that the segment rises above the surface. This model neglects elastic anisotropy and image forces. Using $L = b = 10^{-3}$ cm, and $D = 10^{-6}$ cm$^2$/sec, we get $\gamma_c = 2\,\text{sec}^{-1}$, in accordance with experimental observations for SMLC.[5,20] For thermotropic LCP the plate separations used in shear experiments are usually very small and there is scant reported experimental data, so tentatively we take $D = 5 \times 10^{-8}$ cm$^2$/sec, $L = b = 1$ μm, and get $\gamma_c = 10\,\text{sec}^{-1}$, approximately the value reported by Reference 6. Similar results have been observed with a mainchain thermotropic LCP in rectilinear oscillatory shear: at a frequency of 10 sec$^{-1}$ with a plate separation of 10 μm and an amplitude of $A = 10$ μm a large number of disclination loops suddenly covers the field of vision when viewing the sample with an optical microscope.[21] The frequency of loop emission by a surface source is estimated using Equation (19):

$$B' = (\gamma - \gamma_c)\frac{b}{L} \tag{20}$$

which gives the number of loops emitted by one source per unit time. For simplicity we assume $L = b$. Details of the loop radius and orientation at the instance of emission and dependence of the source operation on the number of loops already emitted are unknown, so we shall assume that if $\gamma > \gamma_c$ a source consisting of a pinned disclination line segment emits loops of constant radius $r_0$ at a frequency given by Equation (20), and take the initial loop orientation as a constant or as a simple function of $\gamma$. In this section we take $\alpha_0 = \pi/2$, $\pi/4$, and $\pi\gamma_c/(2\gamma)$, as some likely initial orientations. Given the present lack of experimental data or observations it seems reasonable at this time to study the predictions of the simplest possible model.

Assume that a nematic liquid crystal is sheared at constant shear rate $\gamma > \gamma_c$; after transients die out, a constant loop density balance is found between the shrinking loops due to their elasticity and emitted loops due to the surface sources. The effects of increasing shear rate are to modify the retraction dynamics and the frequency of loop emission. The loop retraction is described by convection in the loop size space (**a, b**) while the emitted loop frequency on a per source basis is described by $B'$. Formally, the stationary population loop balance on a per source basis is expressed as a constant flux **J** condition:

$$\nabla \cdot \mathbf{J} = \frac{d}{d\mathbf{a}} \cdot \left( \frac{d\mathbf{a}}{dt} n' \right) + \frac{d}{d\mathbf{b}} \cdot \left( \frac{d\mathbf{b}}{dt} n' \right) = 0 \tag{21}$$

where the space is defined by (**a, b**), **J** is the flux of loops with semiaxes **a** and **b**, $d\mathbf{a}/dt$ and $d\mathbf{b}/dt$ are the convection velocities, and $n'$ is the number of loops per unit length having semiaxes length between $a$ and $a + da$ along **a** and between $b$ and $b + db$ along **b**. We are using a linear density $n$ of loops since as we show in the Appendix, a stationary solution restricts the size space with two unique functions

$a = a(b)$ and $\alpha = \alpha(b)$. Assuming that all the loops are emitted with the same angle $\alpha_0$ when they are convected by the flow, and have initially the same radius $r_0$, the dimensionless constant flux equation is given by:

$$\frac{d\mathbf{a}^*}{dt^*} n + \frac{d\mathbf{b}^*}{dt^*} n = -B[\cos \alpha_0 \mathbf{i} + \sin \alpha_0 \mathbf{j} + \mathbf{k}] \tag{22}$$

where $\mathbf{a}^* = \mathbf{a}/r_0$, $\mathbf{b}^* = \mathbf{b}/r_0$, $n$ is the number of loops per unit length, $\gamma^* = \gamma r_0^2/D$, $B = (\gamma^* - \gamma_c^*)$ is the number of circular loops emitted per unit time of unit radius, $\alpha_0$ defines the initial semiaxis $\mathbf{a}^*$ orientation, and $(\mathbf{i}, \mathbf{j}, \mathbf{k})$ are the unit vectors. In the absence of flow Equation (22) properly reduces to the stationary form of Equation (2). As before $\mathbf{a} = (a_x, a_y, 0)$, $\mathbf{b}^* = (0, 0, b^*)$. As shown in the Appendix, the number of loops per unit length is:

$$n(b) = b(\gamma - \gamma_c)[\sin(\alpha_0)]^{2/3} [1 + (\gamma_b^2 + \cot(\alpha_0))^2]^{1/3} \tag{23}$$

The total number of loops $N$ per source is found by integrating in:

$$N = \int_0^1 n(b^*) db^* \tag{24}$$

The average dimensionless loop perimeter $\langle P^* \rangle$ is found from:

$$\langle P^* \rangle = \frac{1}{N} \int_0^1 P^* n \, db^* = \frac{\sqrt{2}\pi}{N} \int_0^1 n \sqrt{a^{*2} + b^{*2}} \, db^* \tag{25}$$

where $a^*$ is given in terms of $b^*$. The final expressions for $n$, $N$, and $\langle P^* \rangle$ are given in the Appendix. The presence of the loops will modify the viscosity since the flow is doing work in deforming and creating the loops. As a first approximation we neglect the second contribution, and assuming that the loops are suspended in an isotropic Newtonian matrix, the total shear stress $T$ is the sum of the suspending Newtonian fluid contribution $T^s$ and the loop contribution $T^L$:

$$T = T^s + T^L \tag{26}$$

The suspending fluid contribution is $T^s = \eta^s \gamma$, and the loop contribution is estimated by the flow work on the loops as:

$$T^L = CN\Gamma(\langle P \rangle - \langle P \rangle_0) \tag{27}$$

where $\langle P \rangle (\langle P \rangle_0)$ is the average perimeter in the presence (absence) of flow, $C$ is the total number of loop emitting sources per unit volume, and $\Gamma$ is the line tension of a loop. The apparent viscosity is then:

$$\eta = \eta^s + \eta^L \tag{28}$$

where the loops contribution of the viscosity is:

$$\eta^L = \frac{CN\Gamma}{\gamma}(\langle P\rangle - \langle P\rangle_0) \tag{29}$$

In the appendix we indicate how to derive the expression for the calculated dimensionless viscosity per source concentration, $\eta^* = N(\langle P\rangle - \langle P\rangle_0)/\gamma^*$, used in the discussion of results below.

Figure 11 shows the loop density $n$ as a function of $b^*$, for three initial loop orientations and three increasing shear rates, obtained from Equation (23). At low shear rates the density is not affected by the initial orientation, and it increases with increasing $b^*$. At higher shear rates loops nucleated at $\pi/2$ exhibit a higher

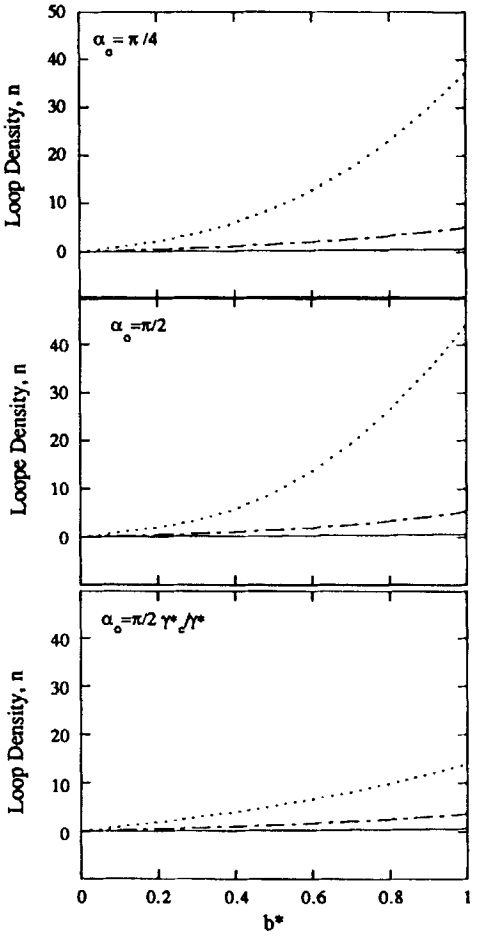


FIGURE 11 Loop density $n$ as a function the semiaxis length $b^*$ for three initial orientations $\alpha_0$: $\pi/4$ (top), $\pi/2$ (middle), $\pi(\gamma_c^* - \gamma^*)/2$ (bottom); the three shear rates $\gamma^*$ are: 1 (full), 3 (dash dot), and 10 (dash).

density than those nucleated at $\pi/4$; the increase is less severe if loops nucleate at smaller angles with increasing shear rates.

Figure 12 shows the corresponding total number of loops per active source $N$ and the average perimeter $\langle P^* \rangle$ as a function of shear rate $\gamma^*$, obtained from Equations (24) and (25), respectively. $N$ increases for the three initial orientations, but the increase is weaker for the case of shear dependent initial orientation. The average perimeters are monotonically increasing for the constant initial orientations but it exhibits a maximum for the shear dependent initial orientation. This can be explained by the presence of two competing effects: larger shear rates increase the frequency of emission of the source but decrease the stretching effect of shear since loops are nucleated closer to the bounding surfaces.

Figure 13 shows the viscosity $\eta^*$, for the three corresponding initial orientations as a function of the shear rate. The viscosity is monotonically increasing for the shear independent initial orientations, indicating shear thickening. The case of shear

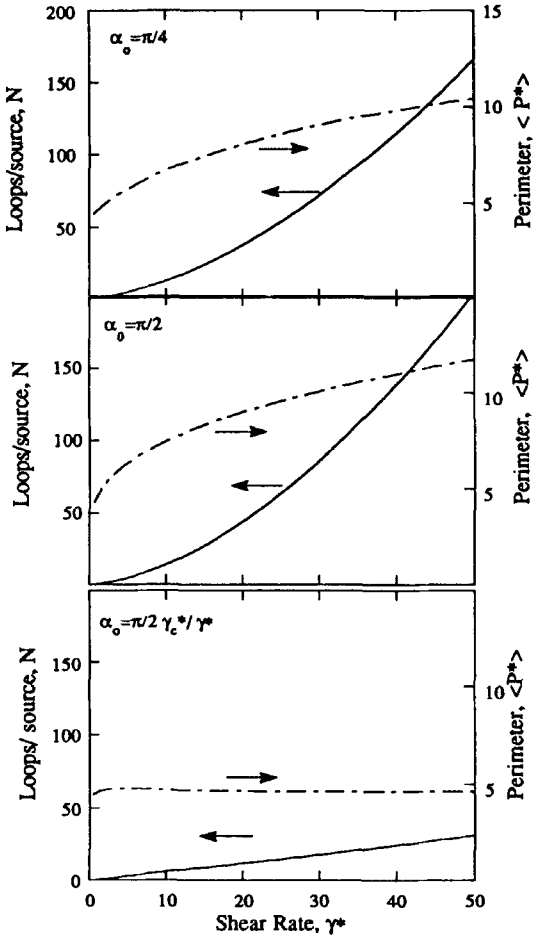


FIGURE 12 Total number of loops per source $N$ and average perimeter $\langle P^* \rangle$ as a function of shear rate $\gamma^*$, for the same initial orientations $\alpha_0$ as in Figure 11.

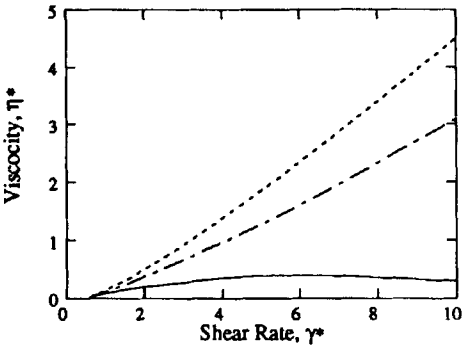


FIGURE 13 Dimensionless viscosity $\eta^*$ as a function of shear rate $\gamma^*$ for three initial orientations $\alpha_0$: $\pi/4$ (dash dot), $\pi/2$ (dash), $\pi(\gamma_c^* - \gamma^*)/2$ full.

dependent initial orientation shows a maximum at a given shear rate, indicating the presence of shear thickening due to large number of loops, and a shear thinning region due to the insensitivity of the average loop perimeter to the strength of shear.

Shear thickening due to large nucleation of disclination loops has been experimentally detected for the case of a lamellar fluid and a model similar to that presented here seems to be consistent with experimental observations.[14] For the steady shear flow of thermotropic nematics undergoing texture changes due to sudden nucleation massive disclination loops at a critical shear rate no data, to our knowledge, is presently available.

In this section we have shown that a simple population model of elastic loops nucleated at a shear dependent rate, that deform, tumble, and shrink, can predict a stationary loop density. The total number of loops is predicted to increase with shear rate, regardless of initial conditions. The effect of the total number of loops is to increase the viscosity due to the extra flow work expended in deforming the loops; the predicted rheological behavior can be shear thickening and/or shear thinning according to the magnitude of the shear rate and the loop orientation at nucleation.

## 6. CONCLUSIONS

In the absence of flow, disclination loops retract, maintaining the initial orientation, with dynamics that are dictated by the orientation diffusivity. The presence of a steady simple shear flow affects the dynamics of loop retraction, since a shear is an extension and a contraction at $\pi/4$ and $3\pi/4$ to the flow direction. The deformation of shear is coupled to the loop orientation, since the vorticity rotates the loops into regions of varying extension or contraction. Loops initially in the extension quadrant are predicted to tumble and elongate in the flow direction, in agreement with experiments,[5] before retracting to a point in a time that increases with shear rate. At sufficiently high frequencies oscillatory shear produces periodic extensions and contractions in an elastic loop, and the retraction mode consists of

periodic oscillations, with decaying amplitude, between an elongated ellipse and a circle. A sufficiently high frequencies loops retract faster than in the absence of flow, in agreement with experiments.[6] The experimentally observed massive nucleation of loops at a critical shear rate can be explained by using a model presented previously in the literature. A simple loop population balance for a suspension of elastic disclination rings in a Newtonian carrier in steady simple shear flow, accounting for the continuous shear dependent nucleation of equally sized loops, deformation and tumbling due to shear, predicts that the total number of loops is an increasing function of the shear rate, in agreement with experiments. The average perimeter of the loops as a function of the shear rate is sensitive to the initial loop orientation. The model predicts shear thickening if the initial loop orientation is independent of the shear rate, but the loop viscosity as a function of shear rate exhibits a maximum when the initial loop orientation decreases with the reciprocal of the shear rate.

## APPENDIX

The loop population balance equation:

$$\frac{d\mathbf{a}^*}{dt} n + \frac{d\mathbf{b}^*}{dt^*} n = -B[\cos \alpha_0 \mathbf{i} + \sin \alpha_0 \mathbf{j} + \mathbf{k}] \tag{22}$$

gives the linear (one dimensional) density of loops, since the three dimensional space $(a, b, \alpha)$ that defines the loops shape $(a, b)$ and orientation $(\alpha)$ is constrained by two equations, as shown below. This means that the loop density is specified using only one coordinate, which in this case is taken to be the length along the neutral direction, $b$. Dotting Equation (22) with the unit triad $(\mathbf{i}, \mathbf{j}, \mathbf{k})$ gives:

$$\frac{da_x^*}{dt^*} n = -B \cos \alpha_0 \tag{A.1}$$

$$\frac{da_y^*}{dt^*} n = -B \sin \alpha_0 \tag{A.2}$$

$$\frac{db^*}{dt^*} n = -B \tag{A.3}$$

Using Equations (A.1–A.3), in conjunction with $a_x^* = a^* \cos \alpha$, $a_y^* = a^* \sin \alpha$, and the semiaxes equations:

$$\frac{da^*}{dt^*} = \gamma^* a^* \sin \alpha \cos \alpha - \frac{a^*}{b^{*2}} \tag{A.4}$$

$$\frac{db^*}{dt^*} = -\frac{b^*}{a^{*2}} \tag{A.5}$$

we obtain the two constaints:

$$a^*(b^*) = (\cos \alpha_0)^{1/3} b^* [1 + (\gamma^* b^{*2} + \cot \alpha_0)^2]^{1/6} \tag{A.6}$$

$$\sin (\alpha(b^*)) = \frac{1}{[1 + (\gamma^* b^{*2} + \cot \alpha_0)^2]^{1/2}} \tag{A.7}$$

and the linear density $n(b^*)$:

$$n(b^*) = B(\sin \alpha_0)^{2/3} b^* [1 + (\gamma^* b^{*2} + \cot \alpha_0)^2]^{1/3} \tag{A.8}$$

The total number of loops $N$, is given by:

$$N = \int_0^1 n(b^*) db^* = B(\sin \alpha_0)^{2/3} \int_0^1 b^* [1 + (\gamma^* b^{*2} + \cot \alpha_0)^2]^{1/3} \, db^* \tag{A.9}$$

The perimeter $P^*$ of an ellipse of semiaxes $a^*$ and $b^*$ is given by:

$$P^* = \sqrt{2}\pi \sqrt{a^{*2} + b^{*2}}$$

$$= \sqrt{2}\pi b^* \sqrt{1 + (\sin \alpha_0)^{2/3} [1 + (\gamma^* b^{*2} + \cot \alpha_0)^2]^{1/3}} \tag{A.10}$$

where we replaced $a^* = a(b^*)$ using Equation (A.6). Finally the average perimeter $\langle P^* \rangle$ is given by replacing Equations (A.8) and (A.10) into Equation (25):

$$\langle P^* \rangle = \frac{\sqrt{2}\pi}{N} \int_0^1 n(b^*) b^* \sqrt{1 + (\sin \alpha_0)^{2/3} [1 + (\gamma^* b^{*2} + \cot \alpha_0)^2]^{1/3}} \, db^* \tag{A.11}$$

In the absence of flow $\gamma = 0$, and assuming that the source remains active the Equations (A.8), (A.9) and (25) reduce to:

$$n_0(b^*) = Bb^* \tag{A.12}$$

$$N_0(b^*) = B/2 \tag{A.13}$$

$$\langle P^* \rangle_0 = 4\pi/3 \tag{A.14}$$

in agreement with the results given in section 2. Finally, the loop contribution to the viscosity $\eta^* = N(\langle P \rangle - \langle P \rangle_0)/\gamma^*$, is calculated using Equations (A.9), (A.11), and (A.14).

## Acknowledgment

The author wishes to thank the McGill University Computing Center for a grant to defray the computational costs of this research and the Natural Sciences and Engineering Council of Canada for operating grant support.



## References

1. M. Kleman, "Points, Lines, and Walls," Wiley, New York, 1983.
2. M. Kleman, *Rep. Prog. Phys.*, **52**, 555 (1989).
3. S. Chandrasekhar and G. S. Ranganath, *Advances in Physics*, **35**, 507 (1986).
4. C. Viney and C. M. Daniels, *Mol. Cryst. Liq. Cryst.*, **196**, 133 (1991).
5. D. G. Graziano and M. R. Mackley, *Mol. Cryst. Liq. Cryst.*, **106**, 103 (1984).
6. N. J. Alderman and M. R. Mackley, *Faraday Discuss. Chem. Soc.*, **79**, 149 (1985).
7. A. D. Rey, *Liquid Crystals*, **7**, 315 (1990).
8. L. Gill, J. Lega and J. L. Meunier, *Phys. Rev. A*, **41**, 1138 (1990).
9. K. F. Wissbrun, *Faraday Discuss. Chem. Soc.*, **79**, 161 (1985).
10. G. Marrucci and P. L. Maffettone, *J. Rheol.*, **34**, 1217, (1990).
11. G. Marrucci, in "Liquid Crystallinity in Polymers," A. Ciferri, ed., VHC, New York, pg. 395, 1991.
12. R. G. Larson and M. Doi, *J. Rheol.*, **35**, 539, (1991).
13. Y. Yamazaki, A. Holz and S. F. Edwards, *Phys. Rev. A.*, **43**, 5463, (1991).
14. P. Oswald and M. Allain, *J. of Coll. and Int. Science*, **126**, 45, (1988).
15. P. G. de Gennes, in "Molecular Fluids," Les Houches Summer School, R. Balian and G. Weil, eds., Gordon and Breach, New York, pg. 377, 1976.
16. P. G. de Gennes, "The Physics of Liquid Crystals," Clarendon, Oxford, 1974.
17. F. B. Hildebrand, "Advanced Calculus for Applications," Prentice Hall, New Jersey, pg. 280, 1976.
18. B. A. Finlayson, "Nonlinear Analysis in Chemical Engineering," McGraw-Hill, New York, pg. 28, 1980.
19. R. W. Lardner, "Mathematical Theory of Dislocations and Fracture," University of Toronto Press, Toronto, pg. 295, 1974.
20. J. Wahl and F. Fischer, *Mol. Cryst. Liq. Cryst.*, **22**, 359, (1973).
21. M. Srinivasarao, private communication.